AC SAF VALIDATION REPORT

Identifier	Name	Satellite(s)
O3M-352	IASI NRT CO	Metop-C

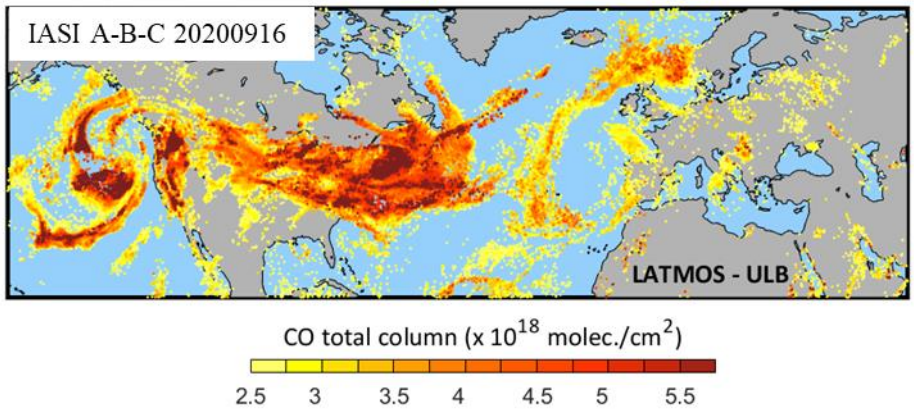

CO total columns from IASI as tracers of cross Atlantic transport of Californian fires

Authors Name	Institute
Bavo Langerock	Royal Belgian Institute for Space Aeronomy
Sarah Safieddine	LATMOS, France
Maya George	LATMOS, France
Cathy Clerbaux	LATMOS/ULB
Daniel Hurtmans	ULB, Belgium
Pierre-François Coheur	ULB, Belgium
Rosa Astoreca	ULB, Belgium

Reporting period:	2008– 2020
Input data versions:	IASI/Metop NRT EumetCAST BUFR_IASI_COx
Data processor versions:	6.005

Table of contents

1. INTRODUCTION

1.1 AC-SAF

Utilising specialist expertise from the Member States, Satellite Application Facilities (SAFs) are dedicated centres of excellence for processing satellite data and form an integral part of the distributed EUMETSAT Application Ground Segment. Atmospheric Chemistry SAF, or AC-SAF, consortium members develop radiative transfer calculation methods and other algorithms for creating atmospheric remote sensing data from polar-orbiting satellites Metop-A, Metop-B, and recently, Metop-C. The AC-SAF produces near real-time data products, validate them and provide associated dissemination and user services. Data is also archived for later access.

1.2 Carbon Monoxide from IASI

Carbon monoxide (CO) is one of the most important precursors of ozone and an important trace gas for the understanding of both air quality and climate forcing. Because of its relatively long lifetime (a few weeks to a few months depending on latitude and time of year), CO is one of the main tracers of long-range transport of pollution. Formed by the incomplete combustion of fossil and bio-fuels, and by vegetation burning, CO is also produced in the atmosphere via the oxidation of methane and non-methane hydrocarbons by the hydroxyl radical (OH). It is the largest global sink of the OH radical and thus plays an important role in the oxidizing power of the atmosphere and in the concentrations of greenhouse gases.

1.3 Purpose and scope

The IASI CO Level 2 products are retrieved in a near real time mode using the Fast Optimal Retrievals on Layers for IASI CO (FORLI-CO) software (Hurtmans et al., 2012), which was developed by ULB in collaboration with LATMOS.

In this document, we will validate the IASI/Metop-C CO product with ground based measurements, and compare this validation with that of IASI/Metop-A and IASI/Metop-B. We also analyze the spatial differences between the three CO products hereafter called IASI-A, IASI-B and IASI-C respectively. The product currently disseminated by EUMETCast is based on the FORLI retrieval algorithm (v20151001, hereafter called FORLI-CO).

This report therefore addresses the quality, stability and the clear continuity of the IASI mission with the IASI-C dataset. As the three instruments (IASI-A, B, and C) are known to be of equal quality and not to suffer from degradation effects, this report inter-compares the IASI-C columns to those of the other two sensors. The two former instruments were extensively validated against other satellite products as well as ground-based observations. It hence follows that by directly comparing the newer instruments, IASI-C, to the former ones, we can indirectly validate this sensor as well.

Two main sections will follow in this Validation Report (VR) to assess the CO IASI products distributed by EUMETCast:

Section 2: Validation of the IASI CO product with ground based measurements (BIRA team)

Section 3: Spatial and temporal inter-comparison between the different IASI instruments (LATMOS/ULB teams).

With the Product User Manual (PUM), the Validation Report (VR) is part of the review material needed for the Operational Readiness Review (ORR).

1.4. Acronyms

BIRA: Royal Belgian Institute for Space Aeronomie
BUFR: Binary Universal Form for the Representation of meteorological data
EUMETSAT: European Organisation for the Exploitation of Meteorological Satellites
EUMETCast: EUMETSAT multi-service data dissemination system
FORLI: Fast Optimal Retrievals on Layers for IASI
FTIR: Fourier Transform InfraRed spectroscopy
IASI: Infrared Atmospheric Sounding Interferometer
LATMOS: Laboratoire Atmosphères, Observations Spatiales
Metop: Meteorological Operational
NDACC: Network for the Detection of Atmospheric Composition Change
NRT: Near Real Time
PUM: Product User Manuel
VR: Validation Report
ULB: Université Libre de Bruxelles
UNS: User Notification System, https://uns.eumetsat.int

1.5. Applicable documents

FORLI-CO Product Specification, Requirement and Assessment
SAF/O3M/ULB/FORLICO_PSRA Issue 1, 21/01/2015
PUM

1.6. References

Buchholz, R. R., Deeter, M. N., Worden, H. M., Gille, J., Edwards, D. P., Hannigan, J. W., Jones, N. B., Paton-Walsh, C., Griffith, D. W. T., Smale, D., Robinson, J., Strong, K., Conway, S., Sussmann, R., Hase, F., Blumenstock, T., Mahieu, E., and Langerock, B.: Validation of MOPITT carbon monoxide using ground-based Fourier transform infrared spectrometer data from NDACC, Atmos. Meas. Tech., 10, 1927-1956, 2017. https://doi.org/10.5194/amt-10-1927-2017

Deutscher, N. M., Griffith, D. W. T., Bryant, G. W., Wennberg, P. O., Toon, G. C., Washenfelder, R. A., Keppel-Aleks, G., Wunch, D., Yavin, Y., Allen, N. T., Blavier, J.-F., Jiménez, R., Daube, B. C., Bright, A. V., Matross, D. M., Wofsy, S. C., and Park, S.: Total column CO2 measurements at Darwin, Australia – site description and calibration against in situ aircraft profiles, Atmos. Meas. Tech., 3, 947–958, https://doi.org/10.5194/amt-3-947-2010, 2010.

Hurtmans, D., P. Coheur, C. Wespes, L. Clarisse, O. Scharf, C. Clerbaux, J. Hadji-Lazaro, M. George, and S. Turquety: FORLI radiative transfer and retrieval code for IASI, J. Quant. Spectrosc. Radiat.Transf., 113, 1391–1408, 2012.

Langerock, B., De Mazière, M., Hendrick, F., Vigouroux, C., Desmet, F., Dils, B., and Niemeijer, S.: Description of algorithms for co-locating and comparing gridded model data with remote-

sensing observations, Geosci. Model Dev., 8, 911–921, https://doi.org/10.5194/gmd-8-911-2015, 2015.

Rodgers, C. D., and Connor, B. J. (2003), Intercomparison of remote sounding instruments, J. Geophys. Res., 108, 4116, https://doi.org/10.1029/2002JD002299, D3.

Ronsmans, G., Langerock, B., Wespes, C., Hannigan, J. W., Hase, F., Kerzenmacher, T., Mahieu, E., Schneider, M., Smale, D., Hurtmans, D., De Mazière, M., Clerbaux, C., and Coheur, P.-F.: First characterization and validation of FORLI-HNO_3 vertical profiles retrieved from IASI/Metop, Atmos. Meas. Tech., 9, 4783-4801,2016. https://doi.org/10.5194/amt-9-4783-2016

Vigouroux, C., Langerock, B., Bauer Aquino, C. A., Blumenstock, T., Cheng, Z., De Mazière, M., De Smedt, I., Grutter, M., Hannigan, J. W., Jones, N., Kivi, R., Loyola, D., Lutsch, E., Mahieu, E., Makarova, M., Metzger, J.-M., Morino, I., Murata, I., Nagahama, T., Notholt, J., Ortega, I., Palm, M., Pinardi, G., Röhling, A., Smale, D., Stremme, W., Strong, K., Sussmann, R., Té, Y., van Roozendael, M., Wang, P., and Winkler, H.: TROPOMI–Sentinel-5 Precursor formaldehyde validation using an extensive network of ground-based Fourier-transform infrared stations, Atmos. Meas. Tech., 13, 3751–3767, https://doi.org/10.5194/amt-13-3751-2020, 2020.

2. COMPARISON AGAINST NDACC FTIR PROFILE DATA

This chapter compares the IASI Near Real Time (NRT) CO product against ground based FTIR measurement data available from the NDACC (Network for the Detection of Atmospheric Composition Change) during the 4-year period 2017 – 2020. Twenty-two sites provide CO profile data see Figure 2.1 and Figure 2.2.

These ground-based, remote-sensing instruments are sensitive to the CO abundance in the troposphere and lower stratosphere, i.e. between the surface and up to 20 km altitude. NDACC CO data is reported on NDACC in GEOMS hdf files which contain amongst others the retrieved CO VMR profiles between the surface and the top of the atmosphere (TOA), averaging kernels and *a priori* profiles. A description of the FTIR instruments and retrieval methodology can be found at http://nors.aeronomie.be. The typical uncertainty on the FTIR CO column is approximately 3% and increases to 7% at high latitude sites. Figure 2.1 provides an overview of all NDACC CO data for the mentioned time period as column-averaged dry-air xCO (xCO is obtained from the reported surface pressure following Deutscher *et al.*, 2010). Paramaribo has outlying surface pressure values causing the xCO to be abnormal although the actual CO profiles are of good quality. All FTIR spectrometers are Bruker type spectrometers, except the instrument at Toronto which is a Bomen spectrometer. For further details on the instruments for each station, we refer to Vigouroux *et al.*, 2020.

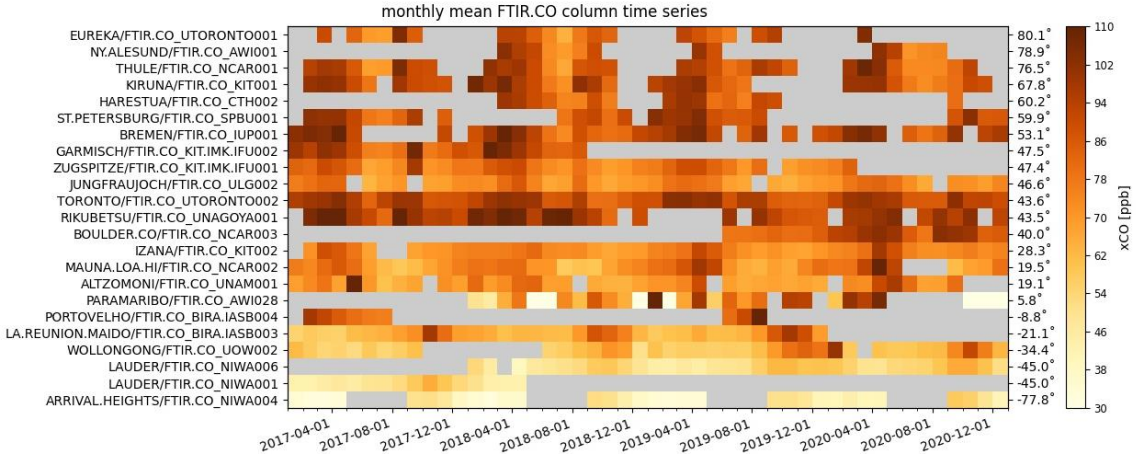

Figure 2.1 Overview of NDACC instruments with CO measurement data in 2017-2020. Time series shows column dry averaged xCO and instruments are labelled by site, institute and number (left) and are sorted by latitude (indicated on the right). FTIR measure direct sunlight and hence no measurements are available at high latitude stations during local winter.

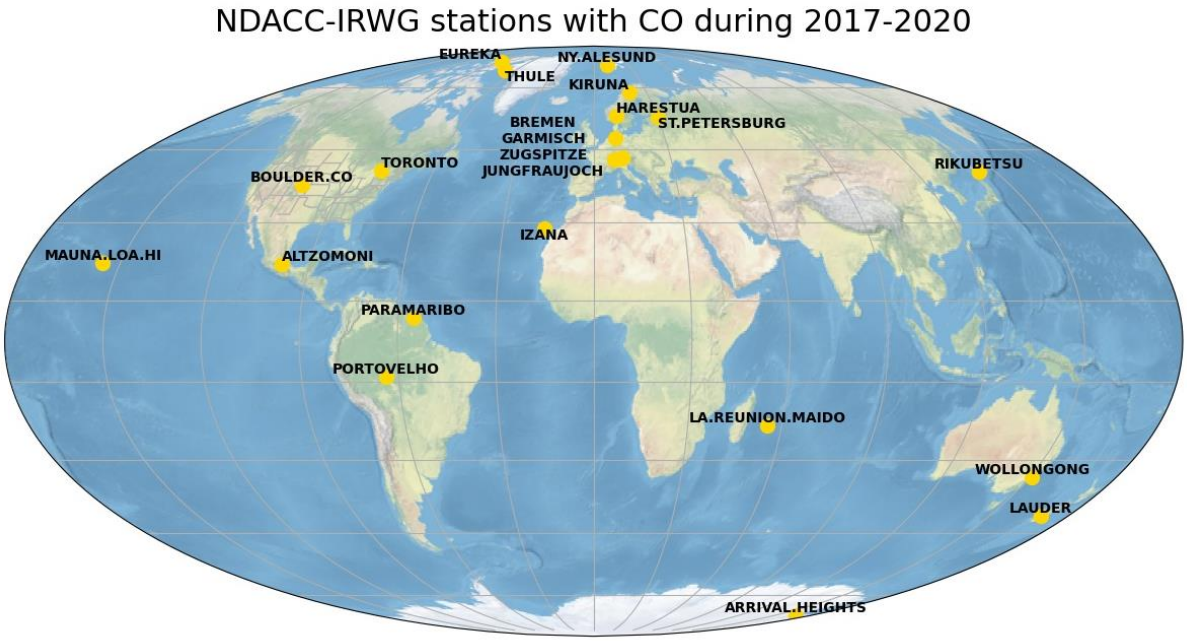

Figure 2.2 World map showing the 22 NDACC stations with CO data during the period 2017-2020.

2.4. Methodology

Each FTIR measurement is co-located to all IASI measurements within a time difference of 3 hours and within a distance of 50 km to the effective location of the FTIR measurement (this effective location is derived from the line of sight of the FTIR measurement). For each co-located pair consisting of a single FTIR and IASI measurement, a sequence of operations is performed aiming to reduce the influence of the two *a priori* profiles used in both the FTIR and IASI retrieval methods (Rodgers *et al.*, 2003). First, the IASI *a priori* is regridded to the FTIR retrieval grid and substituted in the FTIR retrieval following the method described in Rodgers *et al.*, 2003. The second step consists of regridding the FTIR retrieved profile with the IASI *a priori* to the IASI grid and apply the smoothing equation using the IASI averaging kernel, also as described in Rodgers *et al.*, 2003. Regridding is done such that the total mass CO is conserved (Langerock et al., 2014) and possible mismatches between the station surface and the satellite pixel surface are corrected by extrapolation (to go from the IASI grid to the FTIR grid) or by extending the profile by the IASI *a priori* (to go from the FTIR grid to the IASI grid). FTIR profiles containing the IASI *a priori* and which are smoothed with the IASI AVK are referred to as the "smoothed FTIR" profiles (or columns when integrated).

As a final step, all co-location pairs that originate from a single FTIR measurement are averaged, and this includes both the smoothed FTIR profile (calculated with the co-located IASI AVK) and the IASI profile in each co-location pair. Although the comparison methodology uses IASI profiles, the statistics are performed on total columns derived from these averaged and possibly smoothed profiles between the station's surface to the top of the atmosphere. This choice is related to the possibly reduced vertical sensitivity for the IASI profile data (e.g. the IASI averaging kernel at Thule in Figure 2.3) and ensures a network wide valid comparison method. Only FTIR measurements with at least four co-located IASI profiles are taken into account. This validation methodology was also used in Ronsmans *et al.*, 2016.

An example of the co-location and smoothing operation for a single FTIR measurement is shown in Figure 2.3.

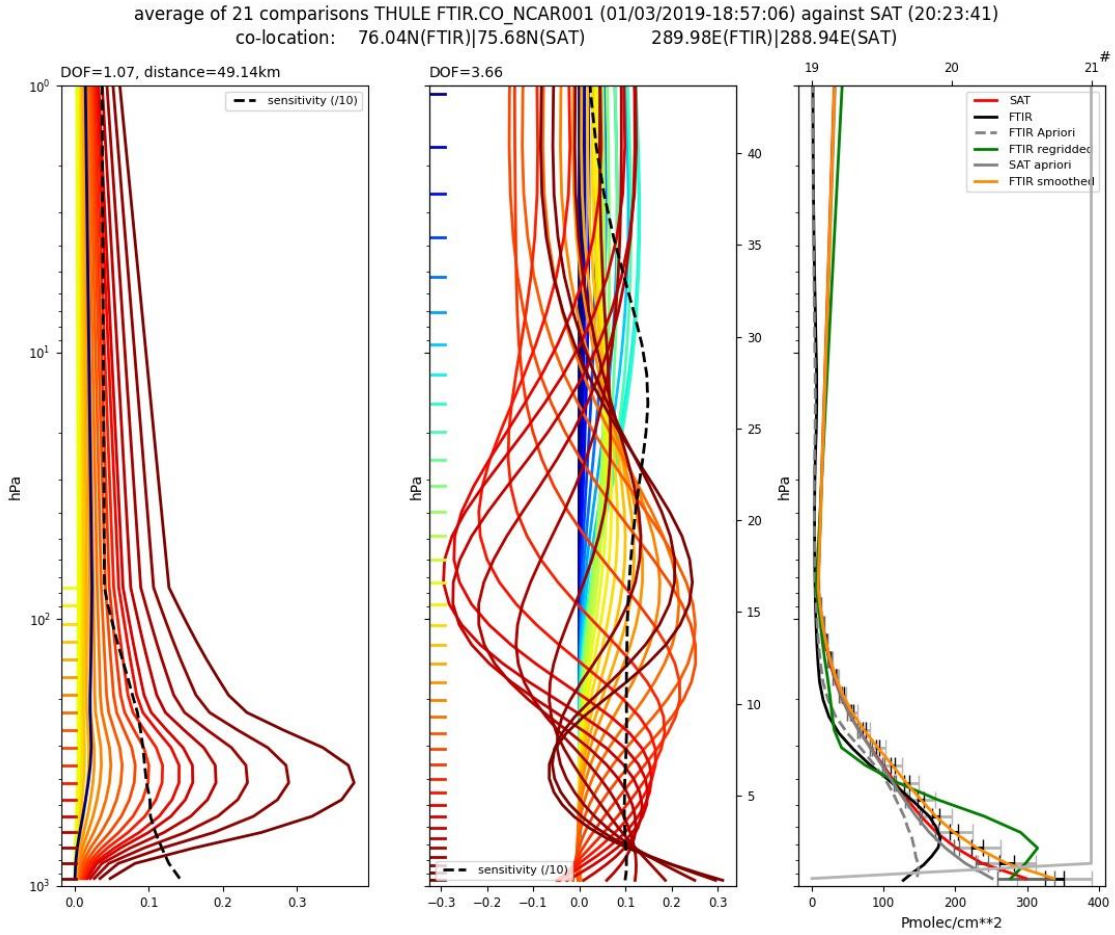

Figure 2.3. A detailed profile comparison plot for a single FTIR measurement against the average of 21 co-located IASI Metop-B retrieved profiles during spring 2019 at Thule (Greenland). The plot consists of 3 panels: the IASI AVK acting on partial column profiles (left), the FTIR AVK acting on partial column profiles (middle) and the partial column profiles considered in the comparison (right). The green profile labelled "FTIR regridded" is the FTIR profile in which the IASI a priori is substituted and regridded to the IASI grid. The smoothing operation will remove the tropospheric gradient as seen in the orange profile labelled "FTIR smoothed". The profiles labelled "FTIR" and "FTIR a priori" are on the finer FTIR grid and should not be compared directly to the partial column profiles on the coarser IASI grid. The FTIR averaging kernel rows corresponding to the lower layers are slightly distorted due to numerical artefacts in the transformation from the state vector units to partial column units.

2.5. Dataset features and comparison statistics.

Statistics are provided using either the smoothed FTIR columns or unchanged FTIR NDACC data.

Table 2.1 and Table 2.2 provide details per station for the relative differences and Pearson correlation coefficients for both the direct comparison and the comparison using the smoothed FTIR columns, respectively. To interpret the statistics, the following remarks on the FTIR data are relevant:

1. Rikubetsu, Ny Ålesund, Paramaribo have only few co-located measurements and are statistically less relevant
2. Measurements at Toronto are done using a Bomen spectrometer and the reported FTIR AVK's have some artefacts that point to an under constrained retrieval. This impacts the smoothed statistics and introduces a systematic bias. This site was not taken into account in the average in Table 2.2. Besides this, the FTIR time-series also seems to suffer from outliers being too low.

IASI NRT data has the following features:

1. During March-April 2018 the IASI-A and IASI-B BUFR files did not contain valid AVK data (see announcement 3719 in the UNS). Figure 2.5 and Figure 2.6 show weird features during this period and is left out in the computation of the statistics for smoothed data in Table 2.2 and in Figure 2.4.
2. The extraction of the CO profiles from the NRT BUFR files takes into account a change in the surface pressure (twt files) scale (date Feb 2 2017) and a unit change in the CO *a priori* and air partial column profile data (date May 15 2019).

Comparison statistics are shown in Tables 2.1 and 2.2 and the Taylor diagrams in Figure 2.4 are representative for the performance averaged over the full time period. Figure 2.5 to Figure 2.7 show the time-series of bi-weekly mean relative differences and represent the performance of the IASI CO data against the entire network throughout the time period 2017-2020. In these figures, red indicates a positive bias (IASI > NDACC) while blue indicates an underestimation of the satellite retrievals. The chosen colour scale is based on the combined FTIR typical uncertainty (3%) and the IASI retrieval uncertainty (4%), so only biases above 5% are to be considered significant (i.e. higher than the combined uncertainties). For both FTIR and IASI measurements, the uncertainties increase at higher latitudes, and biases above 10% should be considered significant for the high latitude stations. All figures for the individual stations can be found on cdop.aeronomie.be.

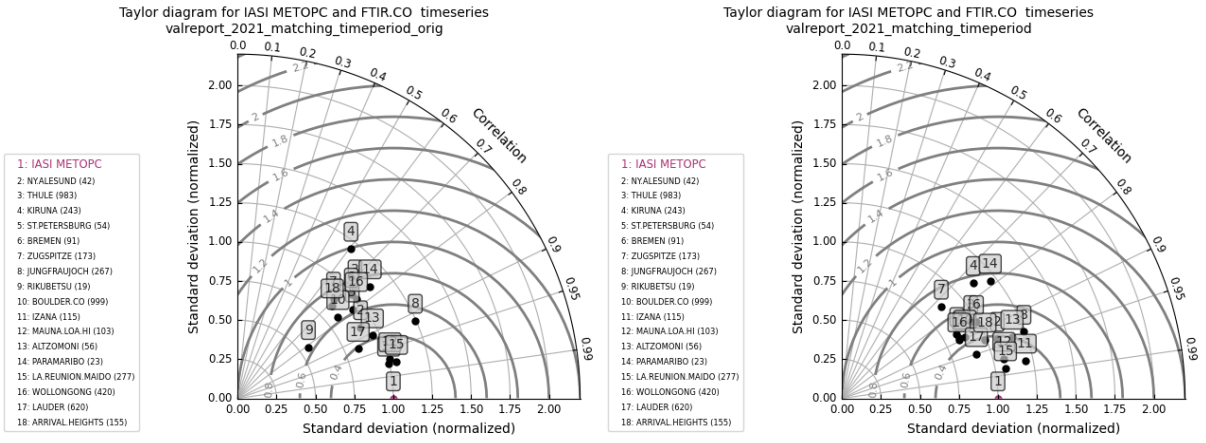

Figure 2.4. Correlation plots for IASI Metop-C direct comparison data (left) and IASI Metop-C smoothed comparison data (right). The Taylor diagram shows the impact of the smoothing operation on the statistics: most correlations shift to values above 0.8.

Table 2.1. Statistics overview for the direct comparison between IASI Metop-B/C and FTIR CO total columns for the entire time period Jan 2017-Dec 2020. The column "std" is the standard deviation of the smoothed FTIR columns relative to the standard deviation of the IASI columns, R is the Pearson correlation coefficient, rel. diff. is the mean of the relative differences IASI minus FTIR in percentage. For 3 sites Harestua, Portovelho and Garmisch no co-locations were found with IASI-C. At Eureka only 2 weeks of measurements co-locate to IASI-C and was left out from the average for IASI-C (indicated in red).

	Metop-B					**Metop-C**				
	# meas.	std.	R	rel. diff.	std. rel. diff.	# meas.	std.	R	rel. diff.	std. rel. diff.
EUREKA	877	0.7	0.73	1.86	14.78	32	0.2	-0.29	-11.44	15.38
NY.ALESUND	82	1.2	0.76	2.22	9.18	42	0.9	0.87	3.71	8.81
THULE	3685	0.8	0.72	-0.34	11.8	983	1	0.73	-0.39	10.26
KIRUNA	676	1	0.66	-2.86	9.6	243	1.2	0.61	-1.57	9.52
HARESTUA	209	1.1	0.86	4.22	6.3	0	nan	nan	nan	nan
ST.PETERSBURG	798	0.9	0.74	0.49	8.58	54	0.9	0.79	0.38	5.74
BREMEN	347	0.8	0.65	0.26	10.59	91	1	0.74	1.66	7.82
GARMISCH	798	0.8	0.72	-7.13	10.85	0	nan	nan	nan	nan
ZUGSPITZE	1638	0.9	0.88	4.69	6.53	173	0.9	0.69	2.74	6.32
JUNGFRAUJOCH	563	1.1	0.88	0.31	4.84	267	1.2	0.92	-1.14	3.93
TORONTO	684	0.7	0.81	5.19	9.66	261	0.7	0.9	4.99	8.42
RIKUBETSU	47	0.7	0.69	-1.14	9.02	19	0.6	0.81	-0.78	7.36
BOULDER.CO	1137	0.7	0.75	-7.81	13.72	999	0.8	0.78	-8.26	12.23
IZANA	573	0.9	0.95	5.74	3.59	115	1	0.97	5.19	3.36
MAUNA.LOA.HI	822	1	0.95	1.15	5.11	103	1	0.97	-0.55	3.52
ALTZOMONI	556	1	0.81	14.39	6.32	56	1	0.91	9.17	5.04
PARAMARIBO	97	0.7	0.9	7.82	6.17	23	1.1	0.77	5.96	4.86
PORTOVELHO	245	0.9	0.97	0.92	7.42	0	nan	nan	nan	nan
LA.REUNION.MAIDO	1721	1	0.98	3.48	4.17	277	1	0.97	5.48	4.46
WOLLONGONG	1213	1	0.83	-0.29	10.08	420	1	0.77	2.57	14.67
LAUDER	1575	0.9	0.94	2.43	6.3	620	0.8	0.93	2.68	6.32
ARRIVAL.HEIGHTS	277	0.7	0.8	9.74	12.33	155	0.8	0.72	7.78	9.77
Averaged for all sites		0.91	0.82	1.91	8.44		0.96	0.82	2.04	7.29

Table 2.2. Statistics overview for the comparison with smoothing between IASI Metop-B/C and FTIR CO total columns for the entire time period Jan 2017-Dec 2020. The column "std" is the standard deviation of the smoothed FTIR columns relative to the standard deviation of the IASI columns, R is the Pearson correlation coefficient, rel. diff. is the mean of the relative differences IASI minus FTIR in percentage. For 3 sites Harestua, Portovelho and Garmisch no co-locations were found with IASI-C. At Eureka only 2 weeks of measurements co-locate to IASI-C and was left out from the average for IASI-C (indicated in red). Smoothed Toronto data suffer from a positive systematic bias and are also left out from the average.

	Metop-B					**Metop-C**				
	# meas.	std.	R	rel. diff.	std. rel. diff.	# meas.	std.	R	rel. diff.	std. rel. diff.
EUREKA	877	0.8	0.89	13.21	13.85	32	0.3	-0.4	10.58	21.29
NY.ALESUND	82	1.3	0.9	14.57	9.1	42	1.1	0.93	19.05	7.78
THULE	3685	0.9	0.87	1.37	9.16	983	1	0.86	2.85	8.04
KIRUNA	676	1.1	0.83	-4.24	7.13	243	1.1	0.75	-3	7.72
HARESTUA	209	1	0.89	6.2	5.77	0	nan	nan	nan	nan
ST.PETERSBURG	798	0.9	0.91	3.14	5.37	54	0.8	0.87	3.51	4.72
BREMEN	347	0.8	0.87	5.77	7.23	91	1	0.87	6.85	6.15
GARMISCH	798	0.9	0.9	-0.01	7.28	0	nan	nan	nan	nan
ZUGSPITZE	1638	1	0.91	-0.48	5.38	173	0.9	0.74	-1.48	5.48
JUNGFRAUJOCH	563	1.1	0.92	-1.06	4.01	267	1.2	0.94	-2.4	3.45
TORONTO	684	0.8	0.78	15.22	12.92	261	0.8	0.92	15.9	8.56
RIKUBETSU	47	0.8	0.84	3.59	6.76	19	0.8	0.89	2.41	5.43
BOULDER.CO	1137	0.8	0.88	-1.85	9.95	999	0.9	0.89	-2.29	9.07
IZANA	573	1.1	0.95	-4.82	3.19	115	1.2	0.98	-5.34	3.25
MAUNA.LOA.HI	822	1.1	0.94	-2.36	5.26	103	1.1	0.97	-4.67	3.25
ALTZOMONI	556	1.2	0.87	6.78	5.27	56	1.2	0.94	1.15	4.39
PARAMARIBO	97	0.9	0.89	9.52	7.24	23	1.2	0.78	6.05	5.3
PORTOVELHO	245	0.8	0.97	6.57	7.1	0	nan	nan	nan	nan
LA.REUNION.MAIDO	1721	1	0.98	0.75	3.86	277	1.1	0.98	2.47	3.55
WOLLONGONG	1213	0.9	0.92	3.03	7.47	420	0.8	0.89	4.72	11.4
LAUDER	1575	0.9	0.96	6.32	5.08	620	0.9	0.95	5.94	5.34
ARRIVAL.HEIGHTS	277	0.8	0.82	11.76	12.03	155	1	0.93	10.11	5.48
Averaged for all sites		**0.95**	**0.90**	**3.70**	**7.02**		**1.01**	**0.89**	**2.70**	**5.87**

2.6. Discussion

From

Table 2.1, Table 2.2 and the Taylor diagrams in Figure 2.4, we learn that the comparison of the smoothed columns increases the overall correlation from 0.8 to 0.9 for IASI-B and IASI-C. Also the ratio of the standard deviations of the two CO column time series FTIR and IASI shift from 0.91 (IASI-B) or 0.96 (IASI-C) to values closer to 1.0. This shows that the smoothing operation reduces the higher variability in the IASI CO time series and increases the correlation.

To compare the performance of IASI-B and IASI-C, the IASI-B statistics should be restricted to October 2019 – 2020 to match the operations period of IASI-C. During the IASI-C operations period, the overall correlation for smoothed IASI-B columns is 0.88, the relative bias is 3.26% and the standard deviation of the relative differences is 6.41%. IASI-C thus performs slightly better compared to IASI-B when considering averaged statistics.

The overall bias for the three years and for all stations is +3% for the smoothed comparison data which is slightly higher than the positive bias of +2% for the direct comparison (Table 2.1 and Table 2.2). In both cases, the overall bias is below the combined uncertainty and is therefore not significant.

At the high latitude sites Eureka, Ny Ålesund and Arrival Heights the overall bias for the smoothed columns is above 10% and this suggests that the IASI CO is overestimated for these sites. For the direct comparison, the biases for the high latitude site are low because the overestimation during summer is not as high and is cancelled by a strong underestimation during local spring.

In fact, the direct comparison reveals that IASI CO is biased low at high latitude sites during local spring (most clearly in the northern hemisphere). This spring underestimation is strongly reduced in the comparison with smoothed columns, which demonstrates that this underestimation is due to a reduced sensitivity in the IASI retrieval at these high latitudes. A detailed comparison is shown in Figure 2.3: the gradient in the FTIR CO profile with higher CO concentration in the free troposphere is removed when applying the IASI averaging kernel and the smoothing operation lowers the FTIR CO column data. Similar during summer where the bias increases because the smoothed FTIR CO columns are lowered when applying the IASI averaging kernel.

Except for the high latitude site, no clear seasonal dependence is revealed in the relative differences for IASI-B. No trend is detected in the time period of 3 years. Because IASI-C follows closely the performance of IASI-B, we expect that similar conclusions can be drawn for IASI-C when the time series covers multiple years.

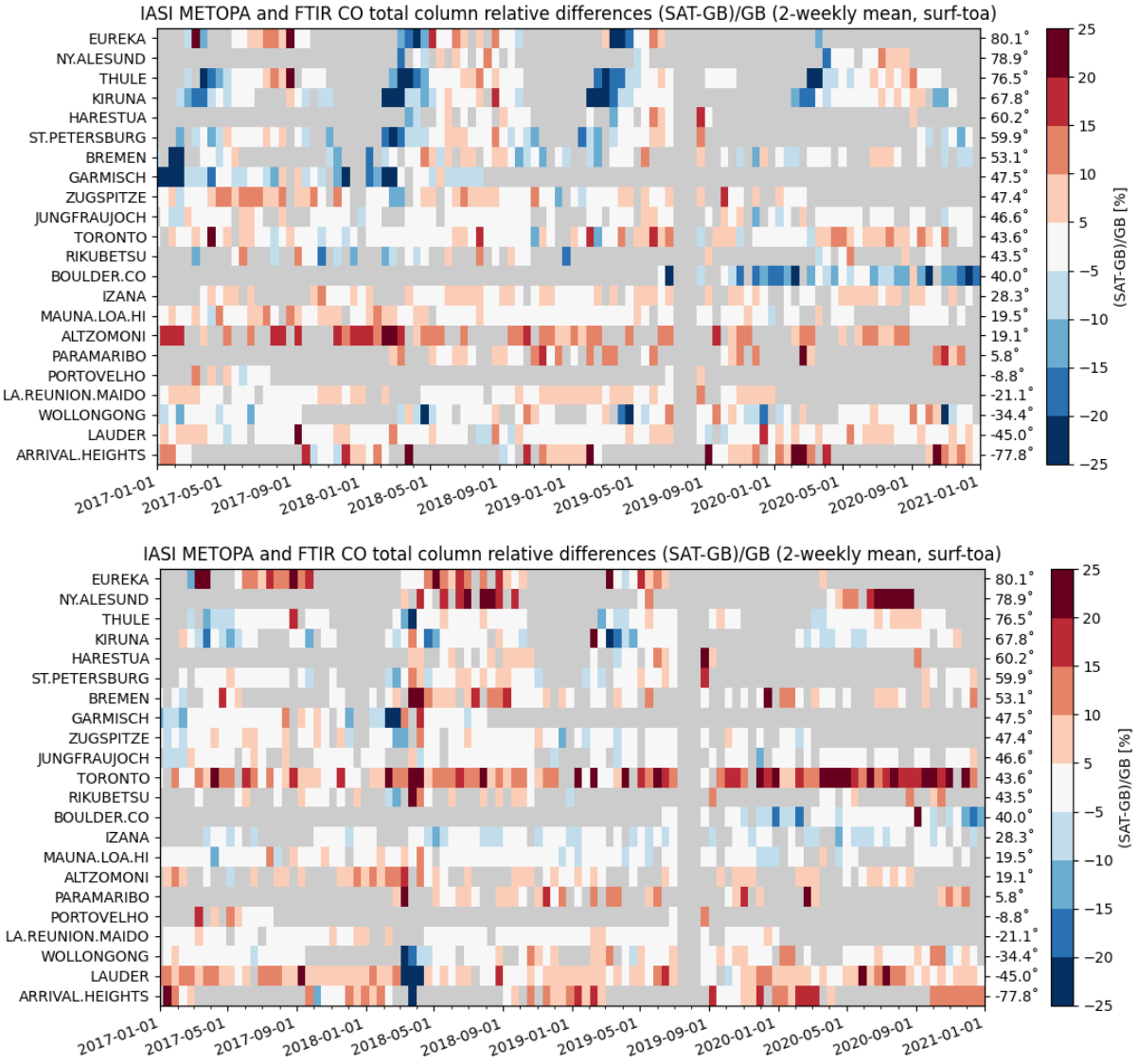

Figure 2.5. Time series of bi-weekly relative difference for IASI Metop-A against NDACC FTIR for the direct comparison (top) and the comparison with smoothing (bottom).

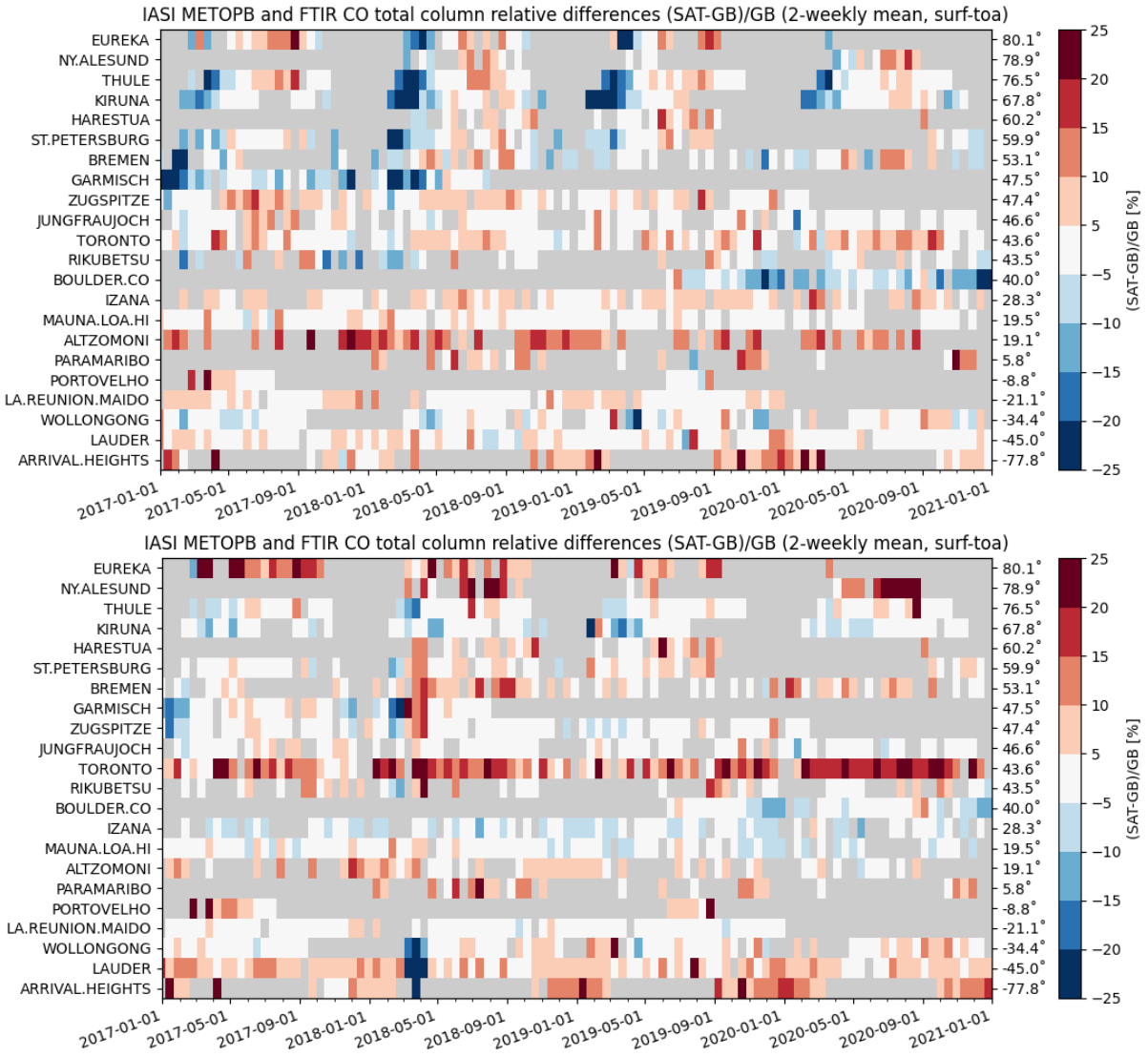

Figure 2.6. Time series of bi-weekly relative difference for IASI Metop-B against NDACC FTIR for the direct comparison (top) and the comparison with smoothing (bottom).

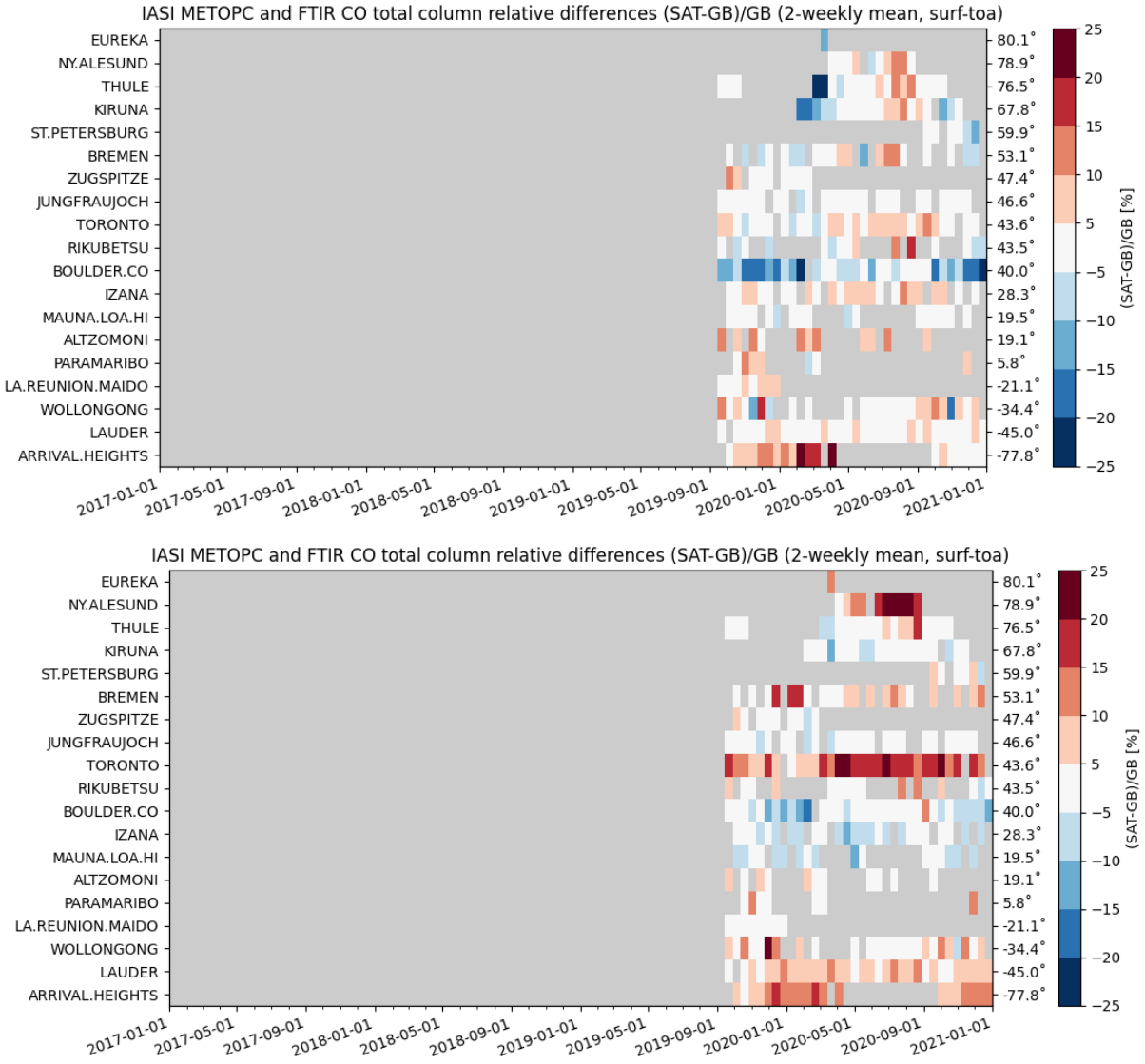

Figure 2.7. Time series of bi-weekly relative difference for IASI Metop-C against NDACC FTIR for the direct comparison (top) and the comparison with smoothing (bottom). Not all stations have co-locations with the IASI Metop-C satellite. Although the Metop-C time series is too short to deduce robust statistics, the time series of the bias corresponds closely to the Metop-A/B time series and the time series shows similar features.

2.7. Acknowledgments

The data used in this report were obtained as part of the Network for the Detection of Atmospheric Composition Change (NDACC) and are publicly available. Data provided by the Royal Belgian Institute for Space Aeronomy (BIRA.IASB, M. De Maziere), Chalmers University of Technology (CTH, J. Mellqvist), Institut fuer Umweltphysik, Universitaet Bremen (IUP, J. Notholt), Karlsruhe Institute of Technology (KIT, M. Schneider, T. Blumenstock), Karlsruhe Institute of Technology - Institute for Meteorology and Climate Research - Atmospheric Environmental Research (KIT.IMK.IFU, R. Sussmann), National Center for Atmospheric Research (NCAR, J. Hannigan), National Institute of Water and Atmospheric Research (NIWA, D. Smale), Saint Petersburg State

University (SPBU, M. Makarova), University of Liege (ULG, E. Mahieu), University of Nagoya (UNAGOYA, T. Nagahama), Universidad Nacional Autonoma de Mexico (UNAM, M. Grutter), University of Wollongong (UOW, N. Jones) and University of Toronto (UTORONTO, K. Strong) was used.

3. SPATIO-TEMPORAL INTER-COMPARISON OF IASI A-B-C

In this section of the report we will show the differences between the three IASI satellites, to show that IASI-C on Metop-C is within the range of the comparison between the other two instruments.

3.4. Spatial differences

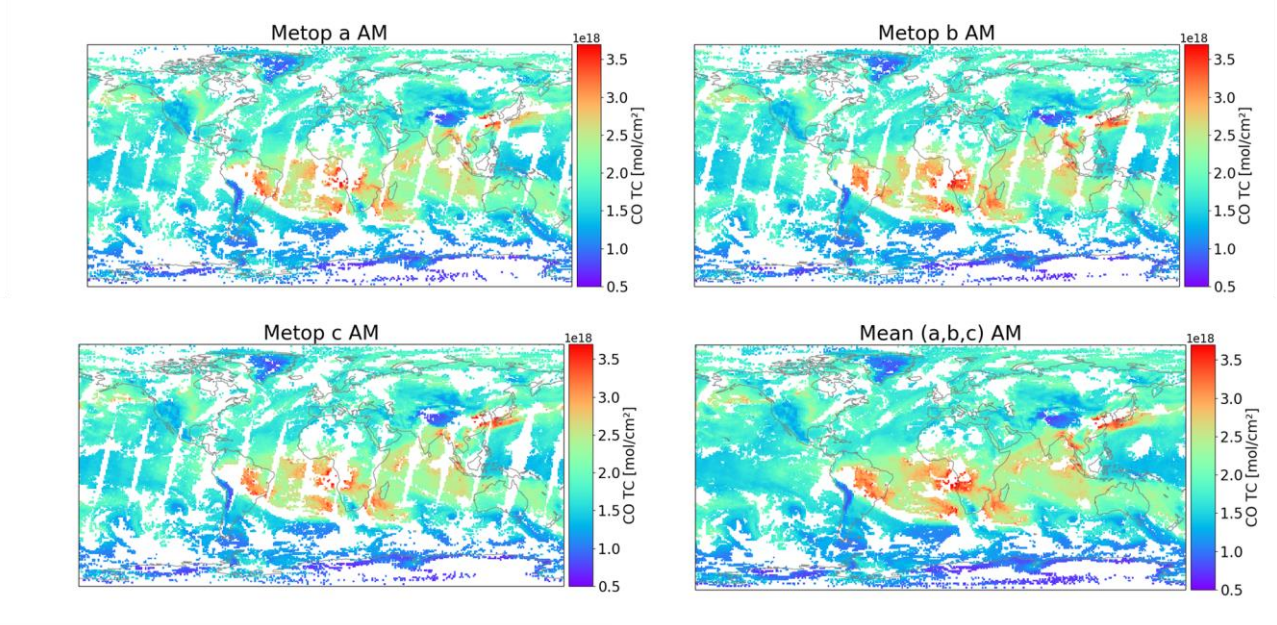

Figure 3.1. 1x1 degree median grids of IASI-A, B, and C daytime observations of October 7 2019, taken as an example. The last panel is the mean of the three Metops.

On a first look, Figure 3.1 shows that the three instruments agree very well spatially, given that the three satellites have similar crossing time (but still around 9:30 AM and PM). The white empty spots on the figure corresponds to cloudy scenes that are discarded during the retrieval. The last panel is the mean of the three Metop satellites. There is a slight added value when taking the mean: as the crossing time is not exactly same the cloud contaminated scenes might have shifted to clear scenes so that the following instrument (whichever comes next from the three), detects CO.

Figure 3.2 shows the spatial difference between the three instruments for the same day used in Figure 3.1. We show the differences between IASI-A and IASI-C (first panel), IASI-B and IASI-A (second panel) and finally IASI-C and IASI-B (last panel). Differences are relatively good, as expected, considering the slight differences in crossing times and fact that every pixel is not covered exactly by every instrument. Larger differences are detected where we have higher CO (Tropics and off the coast of China).

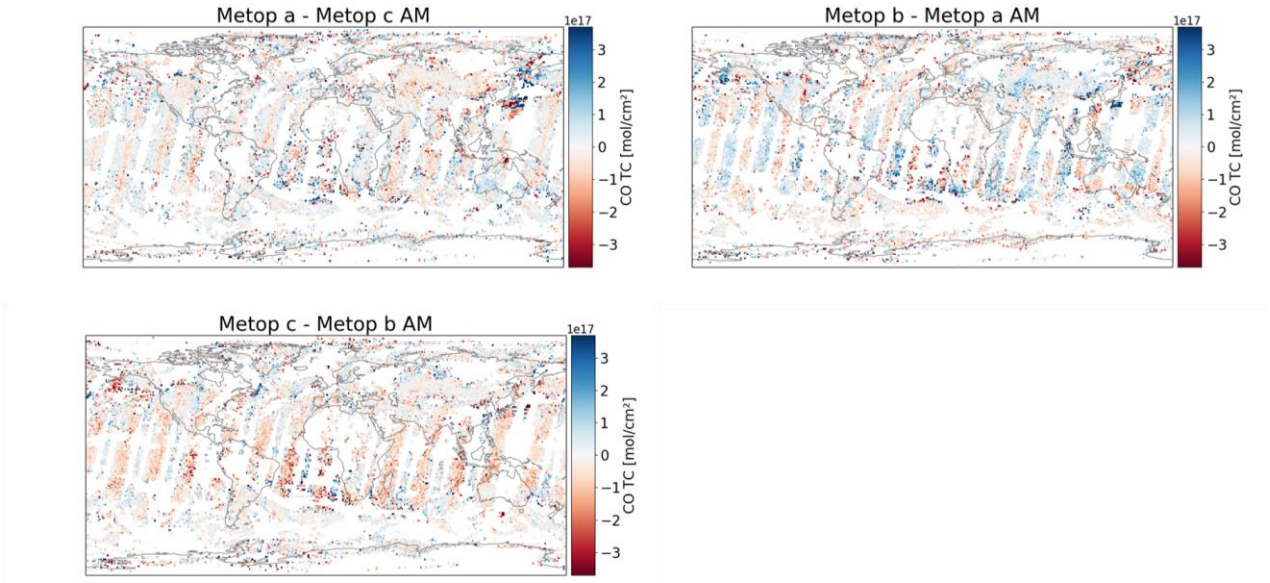

Figure 3.2. CO total column differences on a 1x1 degree grids for the observations shown in Figure 3.1

We note that the difference between IASI-b and IASI-a total columns, in the second panel alternates signs (positive to negative) with orbits. This is due to the time difference between the crossing time of each instrument, which could be +/- one hour. During this time, temperature changes (which are more sensitive to the time of day than the CO itself) will affect the CO restitution and will lead to the changes seen on Figure 3.2.

Figure 3.3 shows the difference between each instrument and the mean of the three instrument (last panel in Figure 3.1). Here we can see that the differences are smoothed by the average and they are very small. More detailed statistical analysis is provided hereafter.

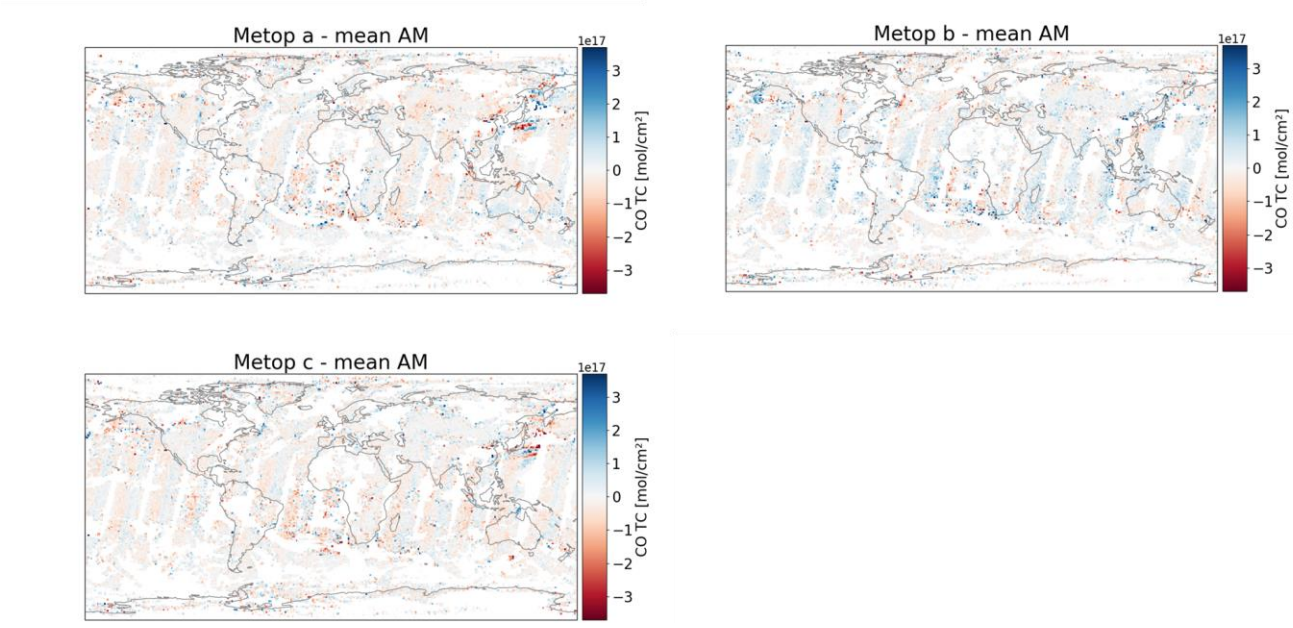

Figure 3.3. CO differences with respect to the mean of the three instruments on 1x1 grid (mean is shown in the last panel of Figure 3.1).

More generally, these three figures show that IASI-C does not show any aberrant observations and is within the differences that are well documented between IASI-A and IASI-B.

3.5. Statistical differences

To quantify the differences, we show here some statistical analysis over the course of few days in September 2019. As an example, the day of 24 September 2019 (day and night observations over 1x1 grid) is show in Figure 3.4.

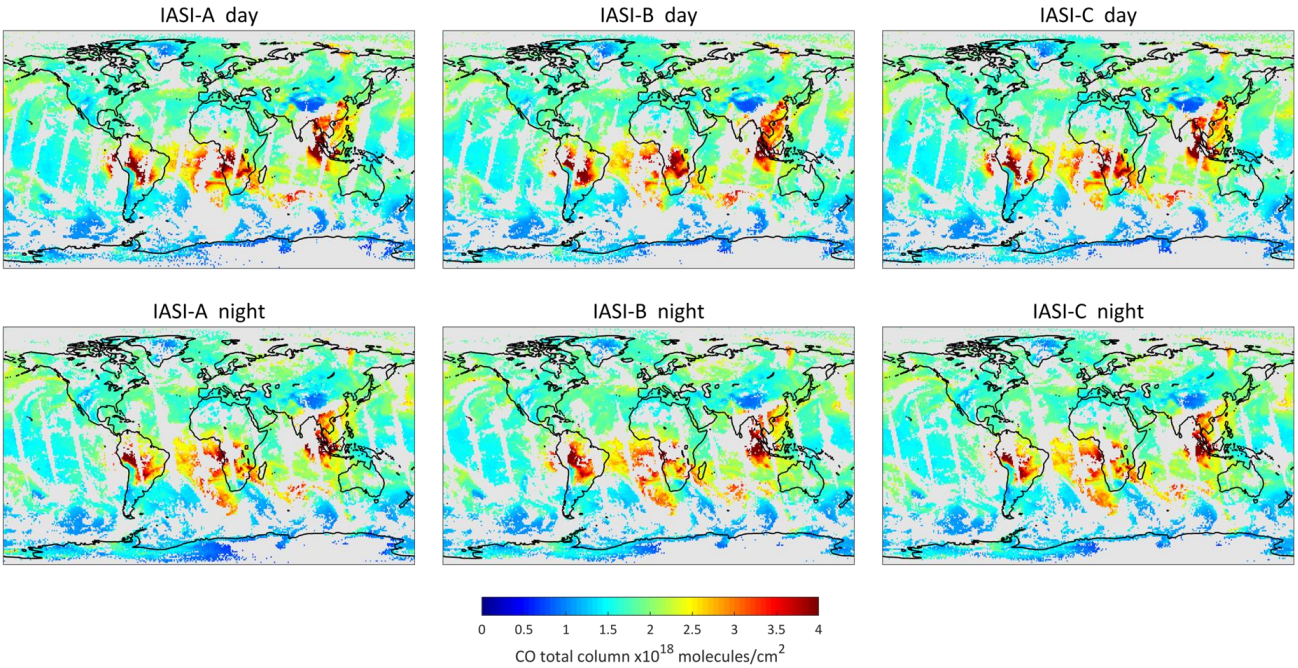

Figure 3.4. Spatial distribution of the CO total columns on 24 September 2019, used for the statistical analysis in Figure 3.5.

Figure 3.4 shows again that the 3 instruments show similar spatial distribution. Since IASI-B at the time of writing of this report is the reference instrument of the IASI mission, we investigate the differences with reference to IASI-B. We show in Figure 3.5 the correlation plots between the reference instrument (IASI-B) and IASI-A and –C (upper panels). We also show the histogram of the biases (lower panels) for the daytime (left) and night-time (right) observations.

Pearson correlation coefficient larger than 0.95 is recorded for all the different sets of instruments. IASI-C seems to correlate slightly better with the reference instrument IASI-B, probably due to the fact that IASI-A has been in drifting orbit since 2017 (as of 2020, the drift is around 40 minutes) leading to a larger difference in the crossing time between Metop-A and Metop-B than those between Metop-B and Metop-C. Another suspected reason might be related to the non-linearity correction applied on board of the different Metop satellites. As it name suggests, the non-linearity might correct differently between the different satellites (in this case leading to better correlation between Metop-B and C than between Metop-A and B).

IASI-C correlation coefficient with IASI-B is very similar during the day and night (0.969 and 0.966). The bias (lower panel) is also more or less the same with a standard deviation of 6.7% and 6.8% for day and night respectively, with an identical absolute bias of 4.9%.

The same analysis was carried for nine other days (for a total of 10 days) and the results are listed in Table 3.1.

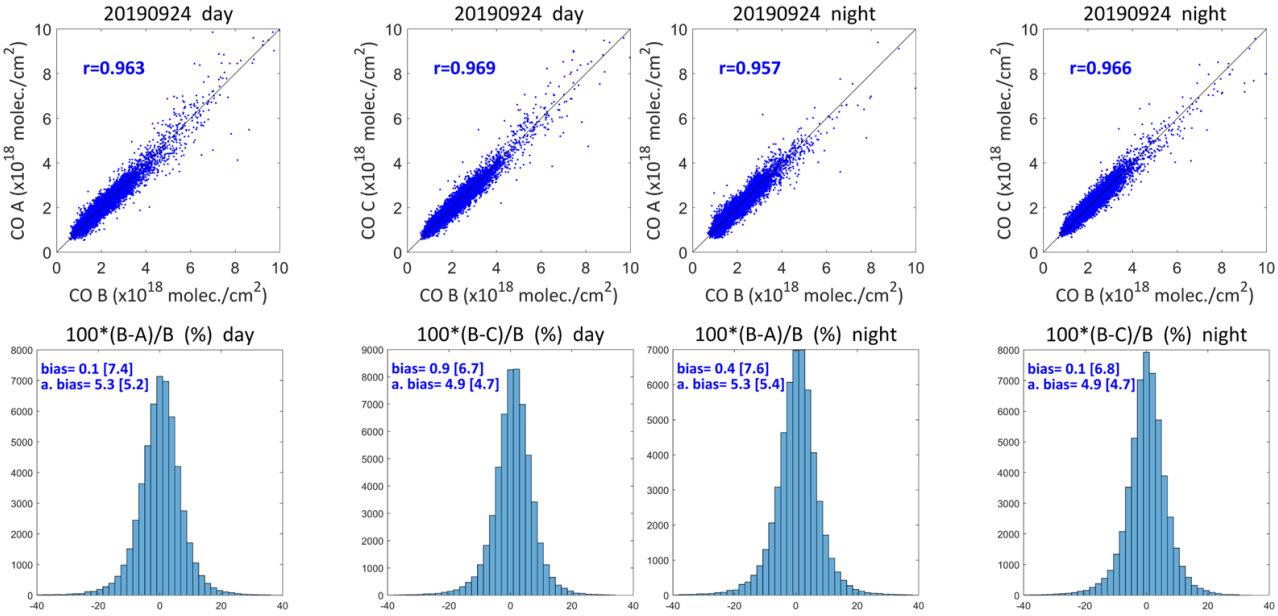

Figure 3.5. Correlation coefficient and histogram of biases between IASI-B (as reference instrument) on one hand, and IASI-A and IASI-B, on the other hand, for daytime (left) and nighttime (right) observations on Sep 24 2019.

Table 3.1. statistical analysis of the correlation coefficient and bias over 10 days in September and October 2019

D=day ; N=night	**20190924**	**20190927**	**20190929**	**20191003**	**20191006**
R (A/B; C/B)	0.96; 0.97 (D)	0.97; 0.97 (D)	0.96; 0.97 (D)	0.96; 0.97 (D)	0.96; 0.97 (D)
	0.96; 0.97 (N)	0.96; 0.97 (N)	0.96; 0.96 (N)	0.96; 0.96 (N)	0.96; 0.96 (N)
Mean Relative Bias [STD] (A/B; C/B)	0.1[7.4]; 0.9[6.7]	0.2[7.3]; 0.8[6.7]	0.3[7]; 0.8[6.5]	0.4[7.4]; 0.9[6.7]	0.3[7.1]; 0.9[6.9]
	0.4[7.6]; 0.1[6.8]	0.5[7.4]; 0.2[6.6]	0.1[7.1]; 0[6.7]	0[7.4]; 0.1[6.7]	0.2[7.2]; 0[6.7]
Mean Absolute Relative Bias [MARB] (A/B; C/B)	5.3[5.2]; 4.9[4.7]	5.2[5.1]; 4.9[4.7]	5.1[4.9]; 4.7[4.5]	5.2[5.2]; 4.8[4.8]	5[5]; 4.8[4.9]
	5.3[5.4]; 4.9[4.7]	5.3[5.2]; 4.8[4.6]	5.1[5]; 4.8[4.7]	5.1[5.3]; 4.8[4.7]	5.1[5]; 4.8[4.7]
D=day ; N=night	**20191008**	**20191011**	**20191015**	**20191018**	**20191021**
R (A/B; C/B)	0.96; 0.96 (D)	0.96; 0.96 (D)	0.95; 0.96 (D)	0.95; 0.96 (D)	0.95; 0.95 (D)
	0.96; 0.96 (N)	0.95; 0.96 (N)	0.94; 0.95 (N)	0.94; 0.95 (N)	0.94; 0.94 (N)
STD (A/B; C/B)	0.1[7.3]; 0.9[6.8]	0.1[7.5]; 0.8[7.2]	0.3[7.2]; 1[6.9]	0.2[7.7]; 0.9[7.2]	0.4[7.4]; 0.9[7.1]
	0.2[7]; 0.1[6.7]	0[7]; 0.1[6.8]	0.1[6.8]; 0.1[6.7]	0[6.9]; 0[6.8]	-0.1[7]; -0.1[7.1]

MARB (A/B; C/B)	5.1[5.2]; 4.8[4.8]	5.3[5.3]; 5.1[5.1]	5.1[5.1]; 5[5]	5.4[5.5]; 5.1[5.2]	5.3[5.2]; 5[5.1]
	5[4.8]; 4.8[4.7]	5[4.8]; 4.9[4.7]	4.9[4.7]; 4.8[4.7]	4.9[4.8]; 4.8[4.8]	5[4.9]; 4.9[5.1]

The data in Table 3.1 shows that what is investigated in Figure 3.5 applies to different days of the year. The correlation coefficient is never less than 0.94; the absolute mean bias is around 5%, and generally the biases are smaller for the IASI-C/IASI-B comparison than that of IASI-A/IASI-B.

3.6. Profile differences

This section aims at comparing CO profiles from IASI-B with IASI-C. The products are both disseminated by EUMETCast in BUFR format (COX). For this study, we looked at profiles above two regions:

Pacific [(-35°, -33°N) ;(-145°, -143°E)] and

Europe [(45°,47°N) ;(3°, -5°E)].

Since there is a time difference between Metop-B and Metop-C measurements, we performed statistics on the mean profiles in 2°x2° boxes/regions delimited by “Pacific” and “Europe” with the longitudes and latitudes listed here. Comparisons are made for twelve days in 2020 (one day per month), for day and night data. Only days with at least ten profiles per instrument were considered.

Tables 1 (for Pacific) and 2 (for Europe) gather the dates, numbers of profiles as well as mean relative biases. Biases are calculated as follows: we calculate the difference between the two mean CO profiles (at each level) and divide by Metop-B CO profile (reference profile). Then we do the mean over the 19 levels of the profile.

Mean relative bias = mean (100(prof_CO_C – prof_CO_B) / prof_CO_B)*

The agreement between IASI-B and IASI-C CO profiles is excellent. For the Pacific region, biases range between -3.22 and 4.97% with an average of 0.18%. Some examples of profiles above the Pacific can be seen in Figures 1 to 3 for March, June and September 15th 2020 (day). For the Europe region, biases range between -4.79 and 4.16% with an average of -0.31%. Some examples of profiles above Europe can be seen in Figures 4 to 6 for June 16th, August 15th and October 18th 2020 (day).

Table 3.2: Relatives biases (column 5) for the Pacific region. Number of averaged profiles for Metop-B and Metop-C are indicated in columns 3 and 4.

		IASI-B #profiles	**IASI-C #profiles**	**Rel. Bias [%]**
20200115	day	46	27	-1.56
20200117	night	25	37	4.97
20200215	day	34	35	0.67
20200215	night	20	26	0.96
20200315	day	17	18	-0.38
20200315	night	22	32	2.61
20200415	day	34	49	-0.81

20200415	night	36	39	0.84
20200517	day	10	28	1.6
20200521	night	25	18	2.04
20200615	day	16	24	-0.17
20200616	night	19	53	0.81
20200715	day	11	44	-2.71
20200716	night	18	15	-2.47
20200814	day	14	19	-1.26
20200815	night	16	14	0.71
20200915	day	25	41	2.08
20200914	night	33	17	-1.32
20201016	day	16	14	-0.77
20201016	night	37	20	1.34
20201114	day	24	24	-2.27
20201114	night	16	11	4.41
20201214	day	42	19	-3.22
20201217	night	27	60	-1.78

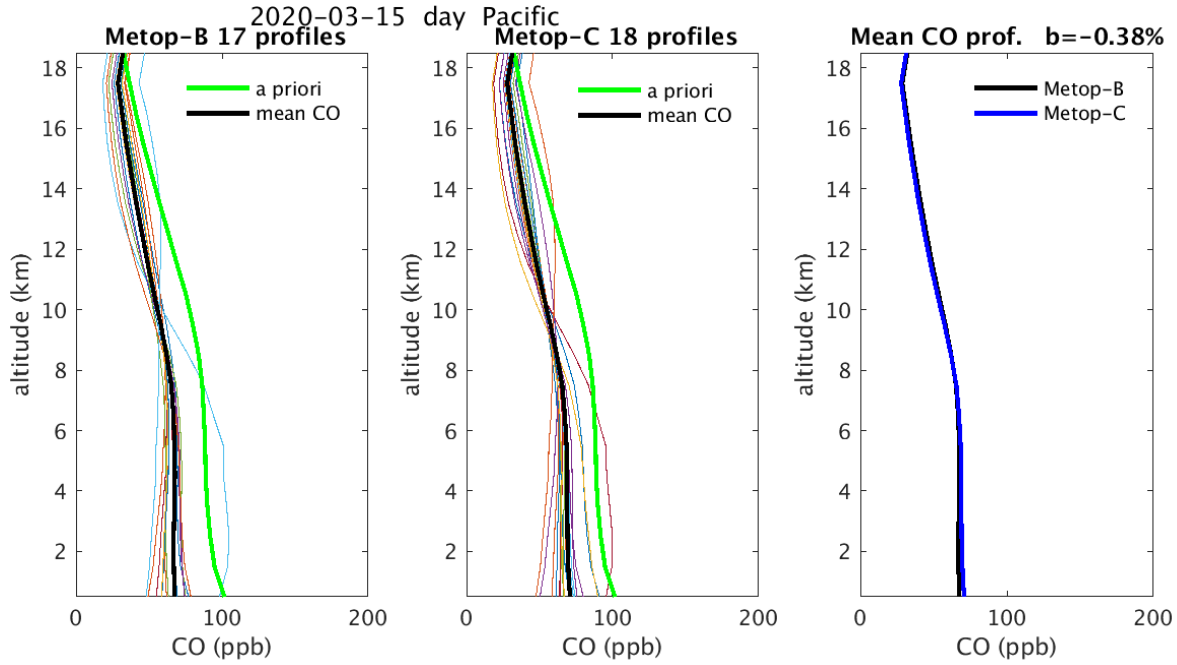

Figure 3.6. Pacific, 2020-03-15. Left: Metop-B profiles in color, mean profile in bold black and apriori profile in bold green. Middle: Same as left but for Metop-C. The two mean profiles are also in the right panel. Relative bias is indicated in the title of right panel.

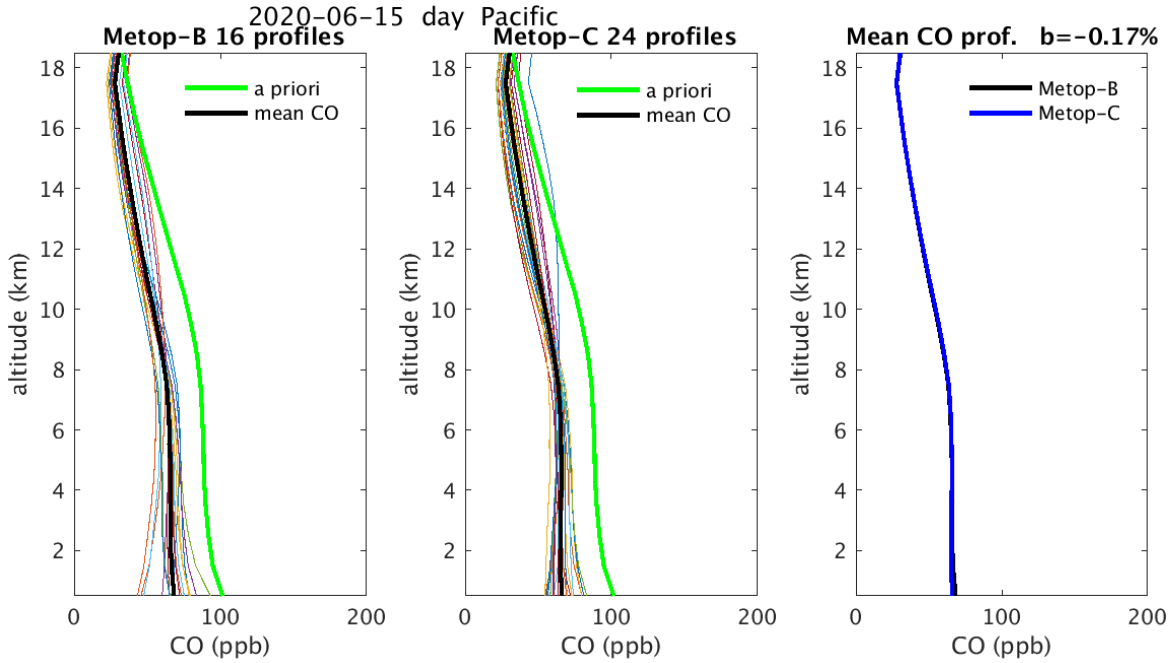

Figure 3.7. Same as Fig. 3.6 but for 2020-06-15.

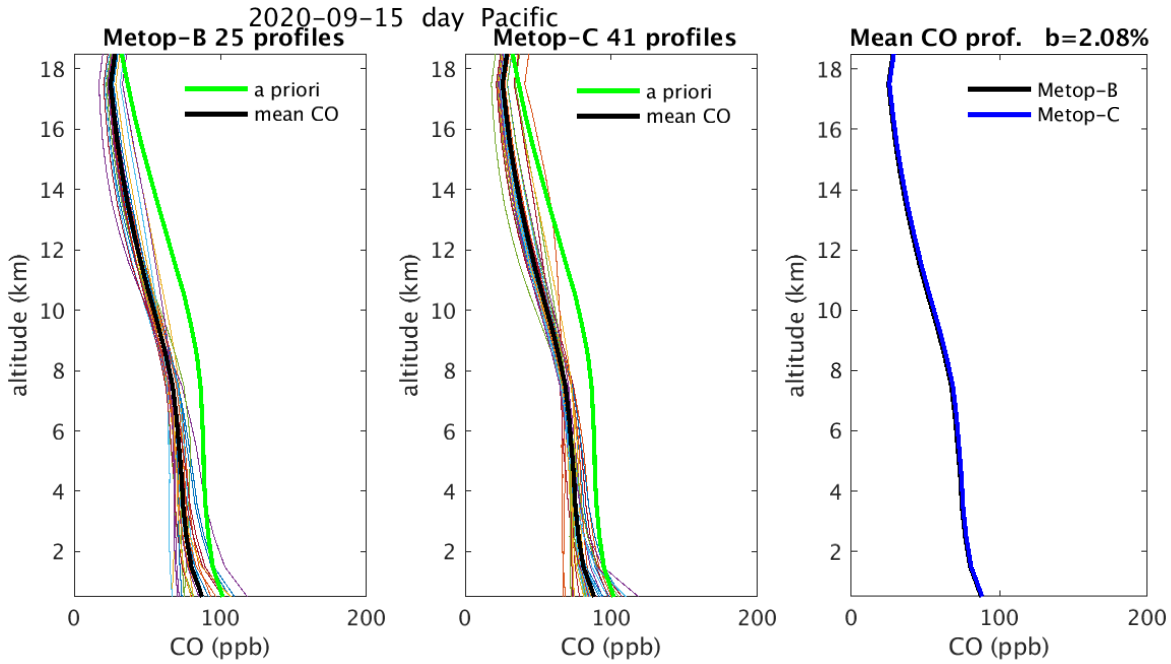

Figure 3.8. Same as Figs. 3.6 and 3.7 but for 2020-06-15.

Table 3.3: Same as Table 3.2 but for Europe.

		IASI-B #profiles	IASI-C #profiles	Rel. Bias [%]
20200116	day	51	34	-3.13
20200116	night	17	35	1.11

20200215	day	38	32	-3.7
20200214	night	27	42	1.51
20200315	day	41	35	-0.39
20200315	night	44	27	-3.43
20200415	day	30	48	2.79
20200415	night	32	38	-1.83
20200516	day	47	35	-0.3
20200516	night	29	36	-0.93
20200616	day	11	14	0.2
20200615	night	22	10	-1.29
20200714	day	12	21	0.14
20200717	night	12	15	-0.15
20200815	day	48	30	4.16
20200815	night	15	15	-0.46
20200915	day	30	39	1.06
20200915	night	47	22	2.34
20201018	day	33	22	0.11
20201018	night	39	35	0.2
20201115	day	41	21	-2.03
20201116	night	22	17	-0.68
20201218	day	28	37	1.94
20201216	night	21	14	-4.79

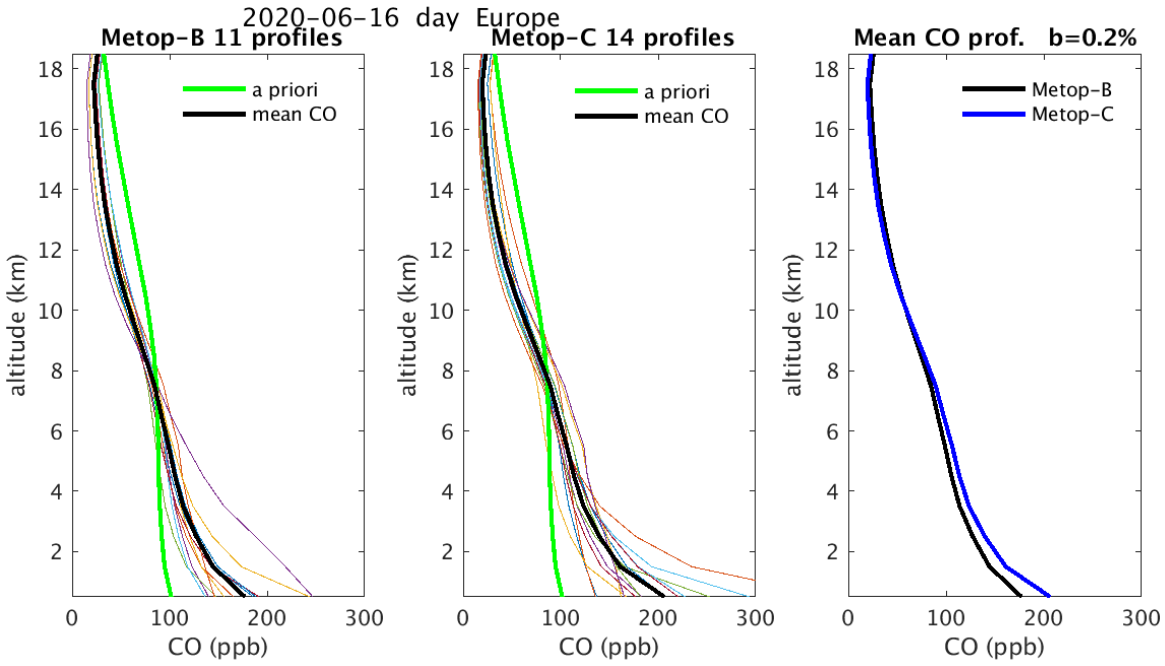

Figure 3.9. Same as Figs 3.6 to 3.8 but for 2020-06-16, over the European region.

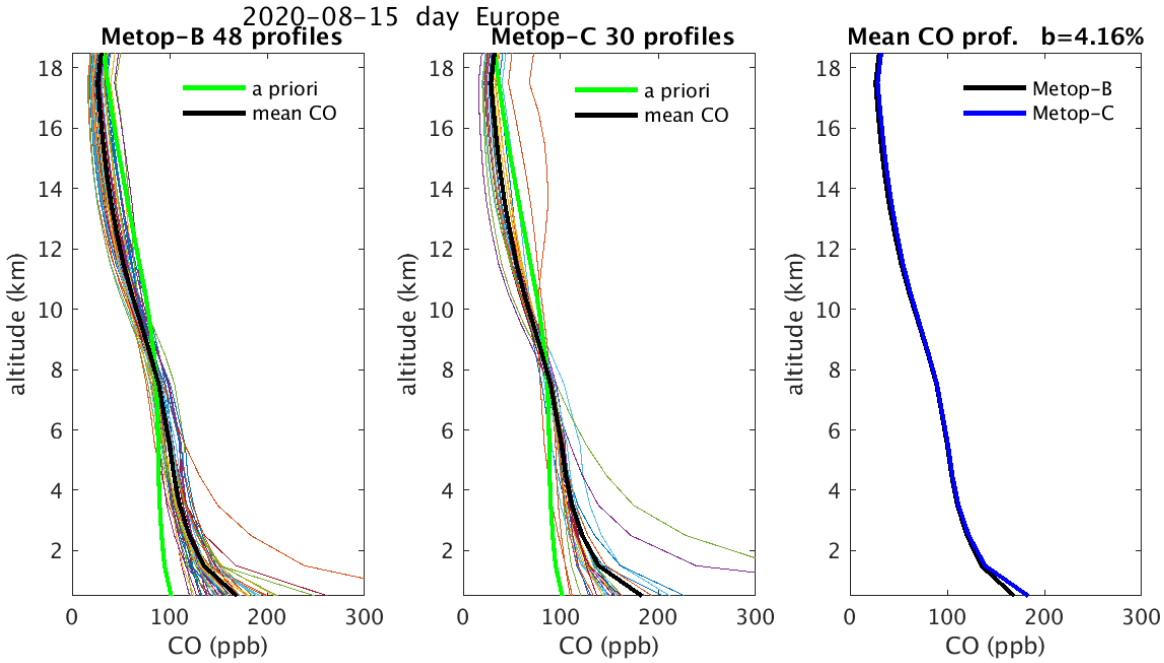

Figure 3.10. Same as Figs 3.6 to 3.9 but for 2020-08-15, over the European region.

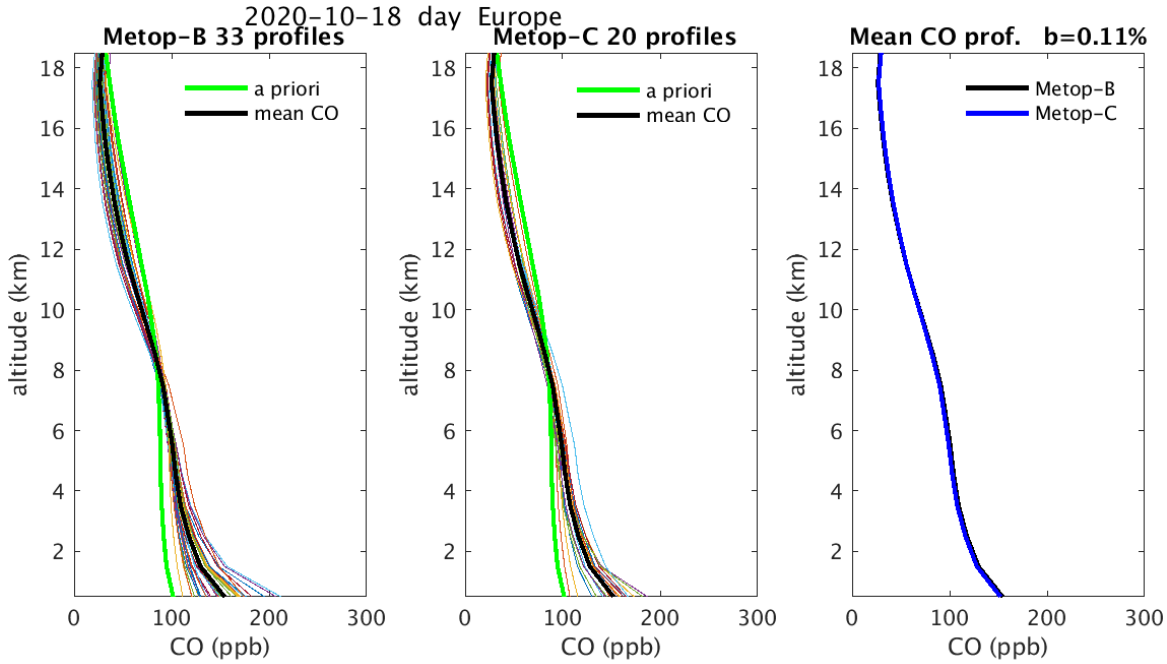

Figure 3.11. Same as Figs 3.6 to 3.10 but for 2020-10-18, over the European region.

3.7. Temporal evolution and stability of IASI-A, IASI-B, and IASI-C

Figure 3.12 shows the temporal evolution of the CO product from IASI since 2008 with the addition of the IASI-B operational product in March 2013 and IASI-C in October 2019.

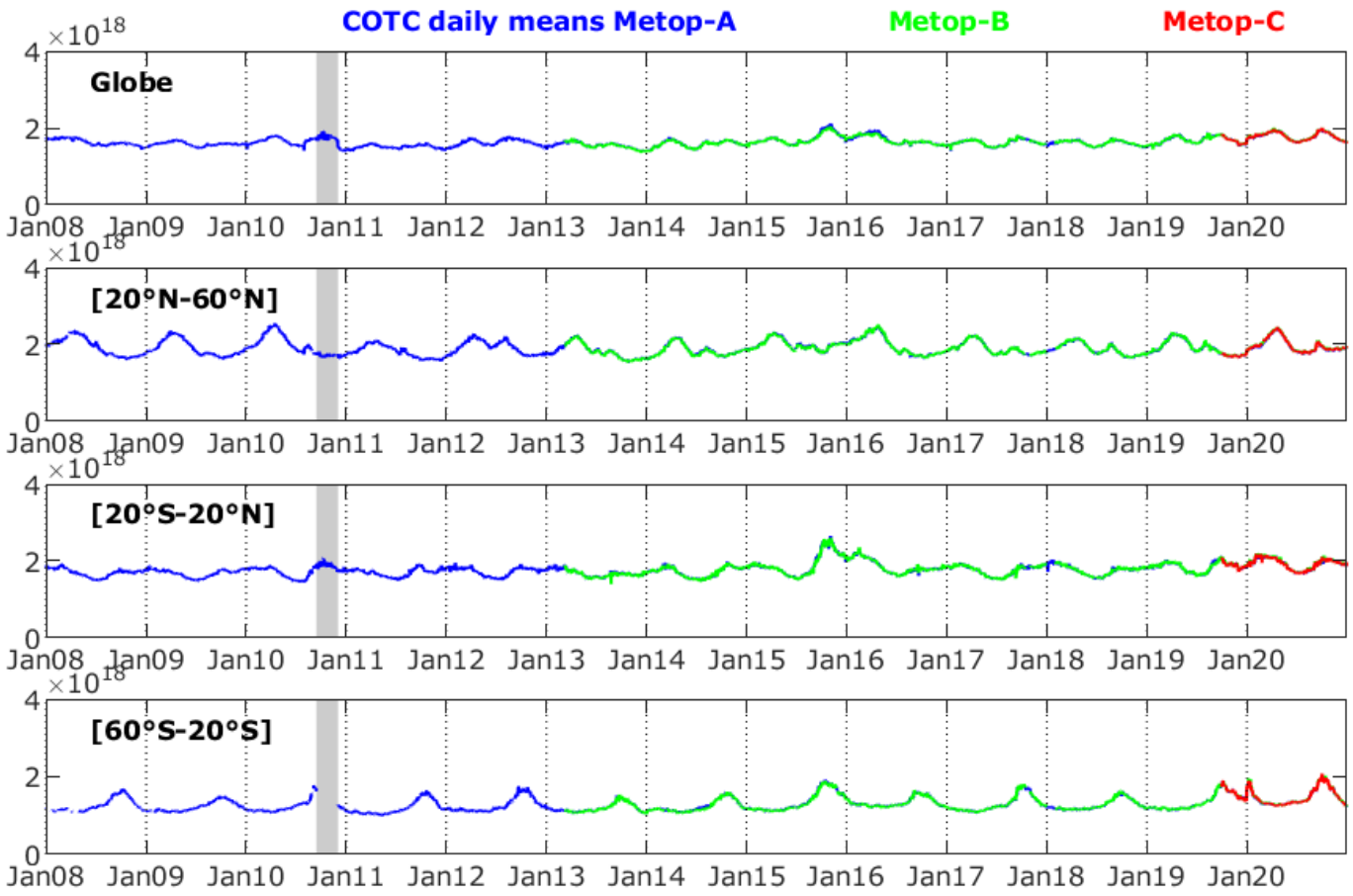

Figure 3.12. Daily (day + night) CO total columns time series (in molecules/cm^2), from January, 1st 2008 until 31 December 2020, for IASI-A in blue, IASI-B in green and IASI-C in red, for the entire globe (top) and different latitude bands. The shaded grey band corresponds to the time period 14/09/2010-02/12/2010 when EUMETSAT only delivered clear sky L2 pixels (i.e. with cloud cover equal to 0): It dramatically reduced the number of FORLI-CO retrieved pixels.

The three products are shown one above the other, and two main points can be deduced:

1- IASI-C ensures the continuity of the mission as it is stable, and agrees very well globally, and on different latitude bands with the other two instruments.
2- The stability of the IASI mission is also clearly shown with no apparent drift to any of the three instruments.

To focus on IASI-C, we show in Figure 3.13 a zoomed version of the upper panel of Figure 3.12 showing the global daily time series of the three instruments in 2020, the first full year with IASI-C observations.

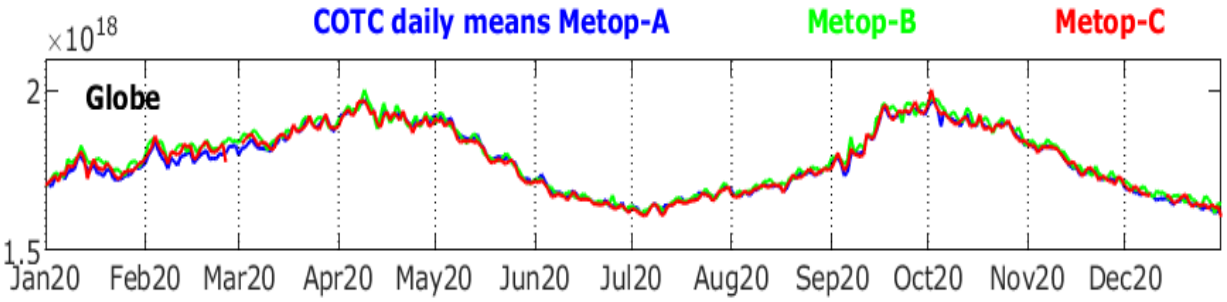

Figure 3.13. 2020 daily (day + night) CO total columns time series for IASI-A in blue, IASI-B in green and IASI-C in red, for the entire globe.

The three instruments agree very well on a daily basis; they show the same seasonal variation corresponding to peaks in the spring (of the Northern and Southern hemispheres).

4. CONCLUSIONS

This validation reports shows that IASI-C ensures well the continuity of the IASI mission. The validation with ground based measurements is within those reported for IASI-A and IASI-B (section 2). Spatial comparison of the CO total column retrievals is in good agreement across the three instruments, and shows excellent correlation between them.

The stability of the 3 instruments is highlighted both in the consistent bias when validating against ground based measurements on one hand, and in the stable time series of the three instruments CO total columns since 2008, on the other hand.

With an average of the relative differences (IASI compared to NDACC stations), of 3.7% (Metop-B) and 2.7% (Metop-C) as mentioned in Table 2.2, **total columns accuracy is below the target of the optimal accuracy (5%) of the FORLI-CO product requirement.**